Photoionization and Recombination

Sultana N. Nahar

Department of Astronomy, The Ohio State University

Columbus, Ohio, USA 43210

Abstract. Theoretically self-consistent calculations for photoionization and (e + ion) recombination are described. The same eigenfunction expansion for the ion is employed in coupled channel calculations for both processes, thus ensuring consistency between cross sections and rates. The theoretical treatment of (e + ion) recombination subsumes both the non-resonant recombination ("radiative recombination"), and the resonant recombination ("di-electronic recombination") processes in a unified scheme. In addition to the total, unified recombination rates, level-specific recombination rates and photoionization cross sections are obtained for a large number of atomic levels. Both relativistic Breit-Pauli, and non-relativistic LS coupling, calculations are carried out in the close coupling approximation using the R-matrix method. Although the calculations are computationally intensive, they yield nearly all photoionization and recombination parameters needed for astrophysical photoionization models with higher precision than hitherto possible, estimated at about 10-20% from comparison with experimentally available data (including experimentally derived DR rates). Results are electronically available for over 40 atoms and ions. Photoionization and recombination of He-, and Li-like C and Fe are described for X-ray modeling. The unified method yields total and complete (e+ion) recombination rate coefficients, that can not otherwise be obtained theoretically or experimentally.

1. Introduction

Although photoionization and recombination are direct opposite processes as they occur in nature, they are usually treated in independent theoretical frameworks. This basic inconsistency, directly related to ionization balance in radiatively ionized media, and consequent inaccuracies, propagate through the photoionization models employed in astrophysics. A further division, largely artificial, is made in theoretical methods used to compute electron-ion recombination rates. Two sets of data are usually calculated: (i) "radiative recombination' (RR), calculated using background, or non-resonant, photoionization cross sections, and (ii) "di-electronic recombination" (DR) representing the contribution of autoionizing resonances, first shown to be important by Burgess (1964). That this procedure is not only theoretically unsatisfactory, but also impractical in most cases, as seen from both theoretical calculations and experimental measurements of photoionization and recombination cross sections. The simple reason is that the resonances are inseparable from the background. The cross sections contain, in general, extensive and interacting Rydberg series of resonances; the non-resonant and resonant contributions are not accurately separable (except, possibly, for few-electron, highly charged ions). The large number of photoionization cross sections computed under the Opacity Project exhibit these features in detail (*The Opacity Project Team* 1995, 1996 - compiled publications and data). In addition, the cross sections for photoionization and recombination of excited states, particularly metastable levels, may contain even more complicated resonances than the ground state (Luo et al. 990). Experimentally, of course, the measurements *always* yield a combined (RR + DR) cross section (albeit in limited energy ranges usually accessible in experimental devices).

Therefore a theoretical method that accounts for both the resonant and the non-resonant recombination in a unified manner is desirable, and has been developed (e.g. Nahar and Pradhan 1994, Zhang et al. 1999), based on the close coupling (CC) approximation using the R-matrix method (Burke and Seaton 1984, Berrington et al. 1987, Hummer et al. 1993) as used in the Opacity Project and the Iron Project (hereafter OP and IP). Photoionization cross sections may be computed essentially for all bound

states, level of excitation $(n, \ell, SL\pi, SLJ\pi)$, energy range, and with energy resolution to delineate resonances. In principle, the cross section for the inverse photo-recombination process is given by detailed balance. However, since recombination takes place to an infinite number of bound states of (e + ion) system, it becomes impractical (and as it turns out, unnecessary) to do so for the very highly excited levels above a certain n-value (chosen to be 10 in practice). For recombination into levels with n>10, the non-resonant contribution, relative to the resonant contribution per unit energy is negligible owing to the density of resonances as n $\longrightarrow \infty$. In that range we employ a precise theoretical treatment of DR based on multi-channel quantum defect theory and the CC approximation (Bell and Seaton 1985, Nahar and Pradhan 1994) to compute the recombination cross section.

Among the problems that manifest themselves in the CC photoionization/recombination calculations are: the accuracy and convergence of the eigenfunction expansion for the ion, relativistic fine structure effects, the contribution from non-resonant recombination into high-n levels as $E \longrightarrow 0; n \longrightarrow \infty$, resolution of narrow resonances with increasing n and/or ℓ, and radiation damping thereof.

Experimental work is of importance in ascertaining the accuracy of theoretical calculations and the magnitude of various associated effects, since most of the photoionization/recombination data can only be calculated theoretically. In recent years there has also been considerable advance in the measurements of (e + ion) recombination cross sections on ion storage rings (e.g. Kilgus et al.1990, 1993, Wolf et al.1991), and photoionization cross sections using accelerator based photon light sources (R. Phaneuf et al., private communication). We compare the CC calculations for both atomic processes with the latest experimental data.

2.   Theory

The CC approximation takes account of the important coupling between the energetically accessible states of the ion in the (e + ion) system. The target ion is represented by an N-electron system, and the total wavefunction expansion, $\Psi(E)$, of the $(N+1)$ electron-ion system of symmetry $SL\pi$ or $J\pi$ may be represented in terms of the target eigenfunctions as:

$$\Psi(E) = A \sum_i \chi_i \theta_i + \sum_j c_j \Phi_j, \tag{1}$$

where χ_i is the target wavefunction in a specific state $S_i L_i \pi_i$ or $J_i \pi_i$ and θ_i is the wavefunction for the $(N+1)$-th electron in a channel labeled as $S_i L_i (J_i) \pi_i k_i^2 \ell_i (SL\pi$ or $J\pi))$; k_i^2 being its incident kinetic energy. Φ_j's are the correlation functions of the $(N+1)$-electron system. Bound and continuum wavefunctions for the (e + ion) system are obtained on solving the CC equations at any total energy E < 0 and E > 0 respectively. The coupling between the eigenfunctions of the energetically inaccessible states of the ion ('closed channels'), and the accessible states ('open channels'), gives rise to resonance phenomena, manifested as infinite Rydberg series of resonances converging on to the excited states of the target ion.

With the bound and the continuum (free) states of the (e + ion) system, atomic cross sections may be calculated for electron impact excitation (EIE), photoionization, and recombination — the free and the bound-free processes. Radiative transition (bound-bound) probabilities may also be obtained.

The R-matrix method, and its relativistic extension the Breit-Pauli R-matrix method (BPRM), are the most efficient means of solving the CC equations, enabling in particular the resolution of the resonances in the cross sections at a large number of energies.

3.   Photoionization

Photoionization calculations are carried out for all levels $(n, \ell, SL\pi, SLJ\pi)$, with $n \leq 10, \ell < n - 1$. Typically this means several hundred bound levels of each atom or ion. The cross section for each level is delineated at about thousand energies, or more, to map out the resonance structure in detail. In recent studies, photoionization cross sections of all ions of C, N, and O were computed (Nahar and Pradhan 1997, Nahar 1998) with more extended eigenfunction expansions, resolution of resonances, and number of levels, than the earlier OP data. Overall, new
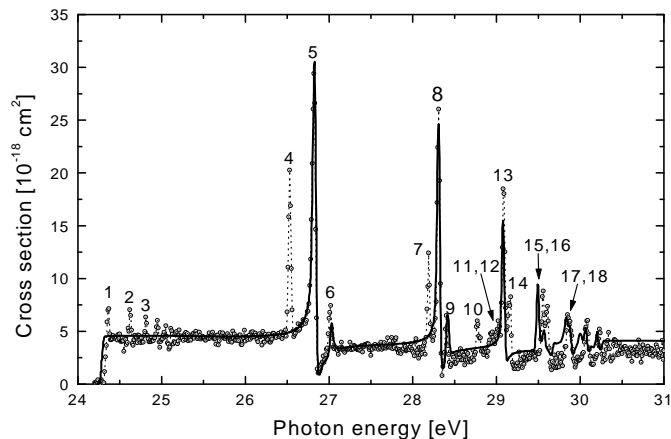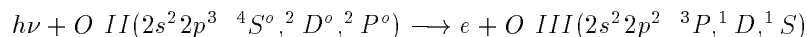
Figure 1.   Photoionization cross sections of the ground state of C II: experiment (open circle, Kjeldsen et al. 1999), theory (solid curve, Nahar 1995)

photoionization data for over 40 atoms and ions, with improvements over the OP data (e.g. currently in TOPbase, Cunto et al. 1993), has now been calculated for: low ionization stages of iron: Fe I, II, III, IV, and V (references in Bautista and Pradhan 1998), Ni II (Bautista 1999), the C-sequence ions (Nahar and Pradhan 1991,1992), the Si-sequence ions (Nahar and Pradhan 1993). Unified (e + ion) photo-recombination cross sections and rates (total and level-specific) have also been obtained, as discussed below.

3.1.   Comparison with experiments

The recent ion-photon merged beam experiment by Kjeldsen et al. (1999) on the photoionization cross sections of the ground state of C II shows an extremely rich and detailed resonance structures (Figure 1). There is excellent agreement between the theory and experiment, both in terms of magnitude and details of the background and resonances. However, the theoretical calculations were in LS coupling, neglecting fine structure, that clearly manifests itself in the additional peaks seen in the experimental cross sections (new relativistic calculations are in progress).

New photoionization experiments have been carried out for positive atomic ions at the Advance Light Source (ALS) in Berkeley, where a photon light source is used on an accelerator that produces the ion beams. These extremely high resolution measurements provide an unprecedented check on the details of the theoretical cross sections, particularly resonance structures and fine structure effects. Figure 2 compares the O II cross section from theory (Nahar 1998), and experiments at the ALS done by the Reno group headed by R. Phaneuf. The experimental cross sections include not only the photoionization of the ground state $2s^2 2p^3$ $\left(^4 S^o\right)$ but also the metastable excited states $2s^2 2p^3$ $\left(^2 D^o, ^2 P^o\right)$.

$$h\nu + O\ II(2s^2 2p^3 \ ^4 S^o, ^2 D^o, ^2 P^o) \longrightarrow e + O\ III(2s^2 2p^2 \ ^3 P, ^1 D, ^1 S)$$

The complicated features arise from several series of resonances converging on to the excited states of the residual ion O III. There is very good agreement between the CC calculations and experiment, verifying the often expressed, but not heretofore established, claim of about 10% accuracy of the theoretical cross sections. The situation may be more complicated, and the uncertainties larger, for more complex atomic systems.

These results also show that metastable states may need to be included in atomic photoionization models of astrophysical sources.
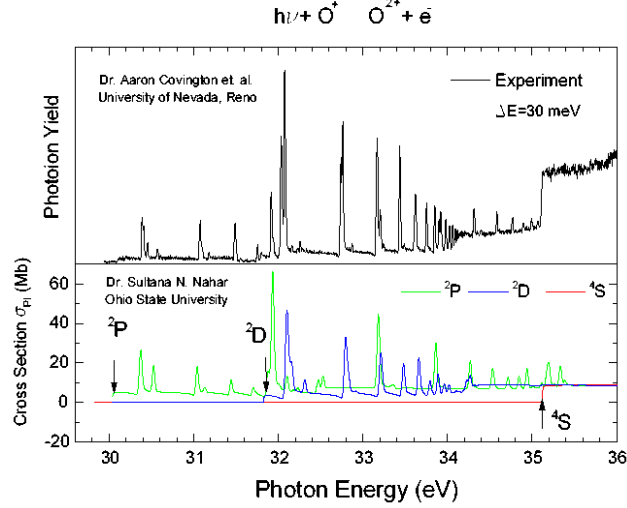
Figure 2.   Photoionization cross sections of the ground and metastable states, $2s^2 2p^3 (^4S^o, {}^2D^o, {}^2P^o)$, of O II: experiment (upper panel, summed σ_{PI}, Phaneuf et al.), theory (lower panel, Nahar 1998). The arrows in the lower panel indicate the threshold cross section for each state.

4.   Unified method for (e + ion) recombination

Photoionization calculations described above are for total photoionization from a given level into all excited levels of the residual ion. However, for photo-recombination the calculations must be repeated to obtain the cross section into the ground state of the ion alone. Detailed balance then applies as

$$\sigma_{RC}(\epsilon) = \frac{\alpha^2}{4} \frac{g_i}{g_j} \frac{(\epsilon + I)^2}{\epsilon} \sigma_{PI}, \tag{2}$$

where $\sigma_{RC}(i_o)$ is the photo-recombination cross section, σ_{PI} is the photoionization cross section into the ground state i_o, α is the fine structure constant, ϵ is the photoelectron energy, and I is the ionization potential in Rydberg atomic units. Recombination can take place into the ground or any of the excited recombined (e+ion) states. The contributions of these bound states to the total σ_{RC} are obtained by summing over the contributions from individual cross sections. σ_{RC} thus obtained from σ_{PI}, including the autoionizing resonances, corresponds to the total (DR+RR) unified recombination cross section in an ab initio manner.

Recombination into the high-n states, i.e. $n_{max} < n \leq \infty$, is computed assuming DR to dominate over the non-resonant background contribution. The CC approximation can then be used to calculate DR collision strengths Ω_{DR}, as an extension of the theory of DR by Bell and Seaton (1985). These two main parts of the unified recombination calculations, and other parts, are described in detail in Zhang et al. (1999). For very highly charged ions, such as the H- and He-like ions with large radiative decay rates for core transitions, radiation damping effects can be significant. As in other CC calculations for excitation and photoionization, resonances are resolved at a suitably fine mesh to enable perturbative radiative damping, and to ensure that the neglected resonances do not significantly affect the computed rates. Relativistic fine structure is considered in the BPRM calculations for highly charged ions.

4.1.   Comparison with experiments

Although experimental results are available for relatively few ions in limited energy ranges, and mostly for simple atomic systems such as the H-like and He-like ions, they are useful for the calibration of theoretical
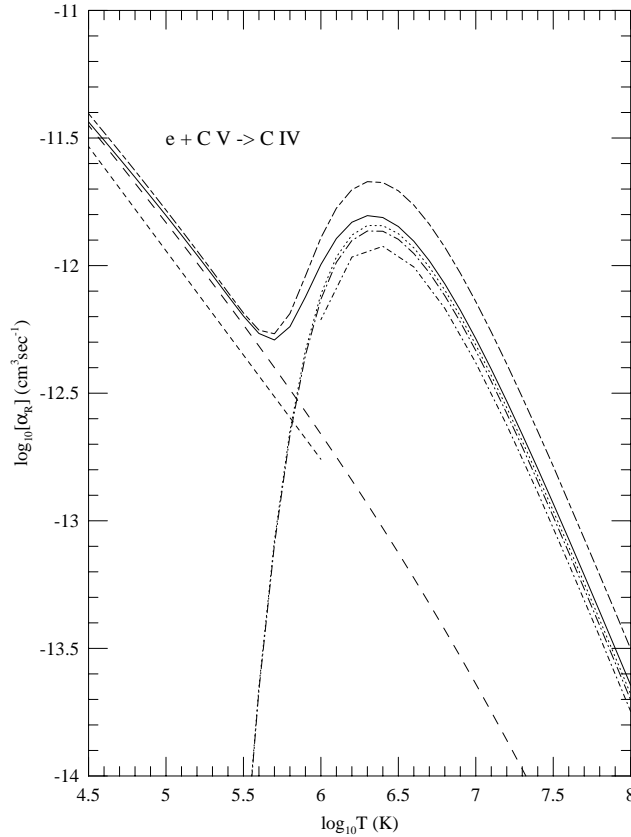
Figure 3. e + C V ⟶ CIV. Total unified rate coefficients: BPRM with fine structure – solid curve, LS coupling – short and long dashed curve; using cross sections from Zhang et al. (1999) – dotted; Savin (1999) – dot-long dash curve; DR rates by Badnell et al. (1990) – dot dash curve; RR rates: Aldrovandi and Pequignot (1973) – short-dash; Verner and Ferland (1996) – long-dash

cross sections. Zhang et al. (1999) have compared in detail the BPRM cross sections with experimental data from ion storage rings for $e + C V \longrightarrow C IV, e + C VI \longrightarrow C V, e + OVIII \longrightarrow O VII$, with close agreement in the entire range of measurements for both the background (non-resonant) cross sections and resonances. The reported experimental data is primarily in the region of low-energy resonances that dominate recombination (mainly DR) with H- and He-like ions. The recombination rate coefficients, α_R, obtained using the cross sections calculated by Zhang et al. agree closely with those of Savin (1999) who used the experimental cross sections to obtain 'experimentally derived DR rates'. However, these rates do not include contributions from much of the low energy non-resonant RR and very high energy regions. The total unified $\alpha_R(T)$ which includes all possible contributions is, therefore, somewhat higher than that obtained from limited energy range. In Figure 3, the solid curve corresponds to the total unified α_R. The dotted curve and the dot-long-dash curves are the rates using cross sections from Zhang et al. (1999) and Savin (1999) respectively, in the limited energy range in experiments (the two curves almost merge). The short-and-long dash curve is the total α_R in LS coupling (Nahar and Pradhan 1997) which, at high temperatures, is higher than the new BPRM rates including fine structure and radiation
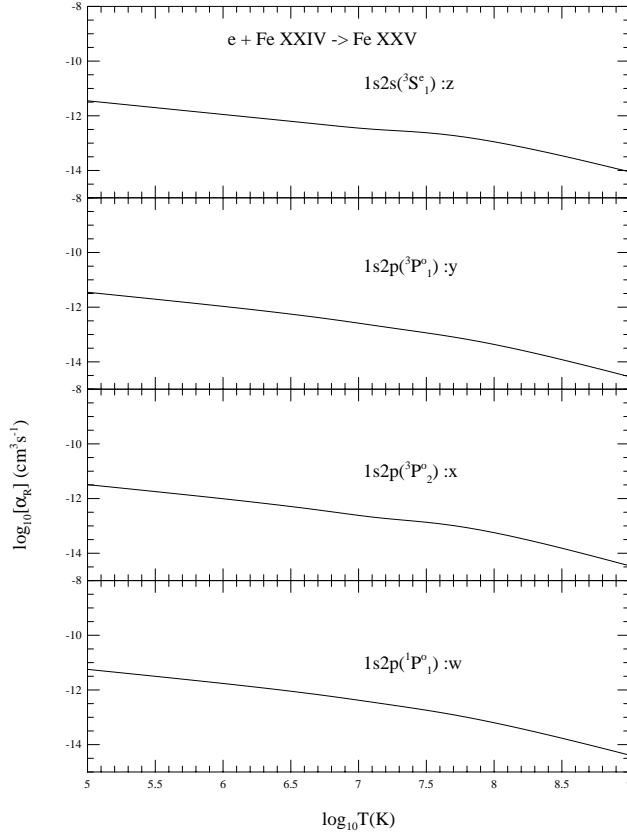
Figure 4.   Level specific recombination rate coefficients for the K-α lines of Fe XXV.

damping (solid curve). The dot-dash curve is the DR rate by Badnell et al. (1990), which is lower than the others. the dashed and the long-dashed curves are RR rates by Aldrovandi and Pequignot (1973), and Verner and Ferland (1996); the latter agrees with the present rates at lower temperatures.

4.2.   Photoionization/recombination of Fe XXV

Fe XXV is one of the most important ions in X-ray spectroscopy (see the review article by Pradhan in this volume). We have completed the calculations for: (i) photoionization cross sections for fine structure levels up to n = 10, including those for ionization into the ground level, and (ii) total and level-specific unified recombination cross sections and rate coefficients.

The most commonly observed lines of Fe XXV correspond to the K-α transitions between the $n=1$ and 2 levels: (1) the 'z' line $1s2s(^3S_1) - 1s^2(^1S_0)$, (2) the 'y' line, $1s2p(^3P_1^o) - 1s^2(^1S_0)$, (3) the 'x' line, $1s2p(^3P_2^o) - 1s^2(^1S_0)$, and (4) the 'w' line $1s2p(^1P_1^o) - 1s^2(^1S_0)$. Recombination rate coefficients into these levels are given in Figure 4; these vary smoothly with temperature, except a slight "shoulder" at high temperature due to DR.

5.   Ionization equilibrium

The new photoionization/recombination data should enable more accurate calculations for photoionization equilibrium

$$\int_{\nu_0}^{\infty} \frac{4\pi J_\nu}{h\nu} N(X^z)\sigma_{PI}(\nu, X^z)d\nu = \sum_j N_e N(X^{z+1})\alpha_R(X_j^z; T), \tag{3}$$

and, coronal equilibrium

$$C_I(T, X^z)N_e N(X^z) = \sum_j N_e N(X^{z+1})\alpha_R(X_j^z; T), \tag{4}$$

where $\alpha_R(X_j^z; T)$ is the total electron-ion recombination rate coefficient of the recombined ion of charge z, X_j^z, to state j at electron temperature T, C_I is the rate coefficient for electron impact ionization, and σ_{PI} is the photoionization cross section evaluated at photon frequency ν and convoluted with the isotropic radiation density J_ν of the source; N_e, $N(X^{z+1})$, and $N(X^z)$ are the densities for the free electrons, and the recombining and recombined ions respectively.

Coronal ionization fractions for C,N,O using the unified recombination rates are also computed (Nahar and Pradhan 1997; Nahar 1999).

6.   Conclusion

We carry out ab initio large scale close coupling R-matrix calculations for (i) photoionization cross sections, and (ii) electron-ion recombination rate coefficients. The predicted theoretical features in σ_{PI} are being observed in the recent sophisticated experiments.

The unified method for (e+ion) recombination has been benchmarked with available experimental measurements. Our study of unified electron-ion recombination rates exhibit a general pattern with temperature. Although generally applicable to all systems, the close coupling unified method is especially suitable for the strong coupling cases where the broad and overlapping resonances dominate the near-threshold region in the electron-ion recombination process, and other methods may not be accurate.

Total and state-specific unified recombination rate coefficients and photoionization cross sections are available for about 40 atoms and ions:
Carbon: C I, C II, C III, C IV, C V, C VI (Nahar and Pradhan 1997)
Nitrogen: N I, N II, N II, N IV, N V, N VI, N VI (Nahar and Pradhan 1997)
Oxygen: O I, O II, O III, O IV, O V, O VI, O VII, O VII (Nahar 1999)
C-like: F IV, Ne V, Na VI, Mg VII, Al VIII, Si IX, S XI (Nahar 1995,1996)
Silicon and Sulfur: Si I, Si II, S II, S III, Ar V, Ca VII (Nahar 2000)
Iron: Fe I (Nahar et al. 1997), Fe II (Nahar 1997), Fe III (Nahar 1996b), Fe IV (Nahar et al 1998), Fe V (Nahar and Bautista 1999), Fe XIII (Nahar 2000), Fe XXIV, Fe XXV (Nahar et al. 2000)
Nickel: Ni II (Nahar and Bautista 2000).

These photoionization/recombination datasets are self-consistent, and should yield more accurate astrophysical photoionization models.

References

Aldrovandi, S.M.V. and Pequignot, D. 1973, Astron. Astrophys. 25, 137.

Badnell, N.R., Pindzola, M.S., and Griffin, D.C. 1990, Phys. Rev. A 41, 2422

Bautista, M.A. 1999, Astron. Astrophys. Suppl. 137, 529

Bautista, M.A. and Pradhan A.K. 1988, Astrophys. J. 492, 650

Bell, R.H. and Seaton, M.J. 1985, J. Phys. B, 18, 1589

Berrington K.A., Burke P.G., Butler K., Seaton M.J., Storey P.J., Taylor K.T., Yu Yan, 1987, J.Phys.B 20, 6379

Burgess, A. 1964, Astrophys. J. 141, 1588

Burke P.G. and Seaton M.J. 1984, J. Phys. B 17, L683

Cunto W C, Mendoza C, Ochsenbein F and Zeippen C J, 1993. A&A 275, L5

Hummer D.G., Berrington K.A., Eissner W., Pradhan A.K, Saraph H.E., Tully J.A., 1993, A&A 279, 298

Kilgus G, Berger J, Blatt P, Grieser M, Habs D, Hochadel B, Jaeschke E, Krämer D, Neumann R, Neureither G, Ott W, Schwalm D, Steck M, Stokstad R, Szmola R, Wolf A, Schuch R, Müller A and Wägner M 1990 Phys. Rev. Lett. 64, 737

Kilgus G, Habs D, Schwalm D, Wolf A, Schuch R and Badnell N R 1993 Phys. Rev. A 47, 4859

Kjeldsen H., Folkmann F., Hensen J.E., Knudsen H., Rasmussen M.S., West J.B., Andersen T., 1999, ApJ 524, L143

Luo D., Pradhan A.k., Saraph H.E., Storey P.J., Yan Y. 1989, J. Phys. B22, 389

Nahar, S.N. 1995, ApJS 101, 423.

— 1996, ApJS 106, 213.

— 1996b, Phys. Rev. A 53, 2417

— 1997, Phys. Rev. A 55, 1980

— 1998, Phys. Rev. A 58, 4593

— 1999, ApJS 120, 131.

— 2000, ApJS 126, 537.

Nahar, S.N., & Bautista M.A. 1999, ApJS 120, 327

— 2000 (in preparation).

Nahar, S.N., Bautista M.A., & Pradhan, A.K. 1997, ApJ 479, 497

— 1998, Phys. Rev. A 58, 4593

Nahar, S.N., & Pradhan, A.K. 1991, Phys. Rev. A 44, 2935

— 1992, Phys. Rev. A 45, 7887

— 1991, Phys. Rev. A 44, 2935

— 1992, Phys. Rev. A 45, 7887

— 1993, J. Phys. B26, 1109

— 1994, Phys. Rev. A 49, 1816

— 1997, ApJS 111, 339

Savin, D.W. 1999, Astrophys. J. 523, 855 *The Opacity Project 1 & 2*, compiled by the Opacity Project team (Institute of Physices, London, UK, 1995,1996)

Wolf A, Berger J, Bock M, Habs D, Hochadel B, Kilgus G, Neureither G, Schramm U, Schwalm D, Szmola E, Müller A, Waner M, and Schuch R 1991 Z. Phys. D Suppl. 21, 569

Verner, D.A. & Ferland G. 1996, ApJS 103, 467

Zhang, H.L., Nahar, S.N., & Pradhan, A.K. 1999, J. Phys. B32, 1459